Production techniques for 3D printed inflatable elastomer structures.

Part I – Fabricating air-permeable forms and coating with inflatable silicone membranes via spray deposition.

Fergal B. Coulter[1,2], Brian S. Coulter, Jason R. Marks, Anton Ianakiev[3]

1. Medical Device Design Group, Department of Mechanical and Materials Engineering, University College Dublin
2. Complex Materials, Department of Materials. ETH Zurich
3. School of Architecture, Design and Built Environment, Nottingham Trent University

Keywords : Inflatable structure, Permeable mandrel, Spray deposition, Balloon Fabrication.

Abstract: This article is the first in a two-part series describing a process for conformal 3D printing on to inflatable substrates. Details for fabricating seamless, tubular elastomeric membranes by spray deposition on a double-curved air-permeable mandrel are presented, in Part I. The mandrels are created by casting gypsum into a desired form, and made permeable by applying pressurised air to the central core of the gypsum body during its crystallisation phase. The membranes — in this case made from silicone — are created by spray deposition onto the mandrel using a constant surface angular velocity approach. These membranes are inflated so as to impart mechanical pre-strain in the rubber by stretching. The techniques described are particularly suited to fabrication of 3D printed Pneumatic Artificial Muscles (PAM) and Dielectric Elastomer Actuators (DEA). They can also be used to create removable substrates upon which a 3D print can be extruded, or alternatively integrated into a 4D print where varying levels of mechanical strain can be distributed through the various printed layers. Uses for the techniques described include soft robotics, stretchable electronics, biomechanical implants and custom bioreactors, particularly when combined with direct ink writing techniques.

Introduction

This article follows on from [1], which is a short description of a novel process to create pre-strained tubular Dielectric Elastomer Minimum Energy Structures (DEMES) entirely though additive manufacturing methods. It is Part I of a series and the intention of these two papers is to describe an additive manufacturing method which can create collapsible, non-buckling minimum energy structures of customisable shape in a repeatable fashion. Silicones of varying hardness were used as the materials to prove the concepts, but the described techniques are not limited to using such. Described is a low-cost method to create air permeable mandrels, upon which, spray deposition is used to fabricate thin silicone elastomer membranes of even thickness. These membranes are inflated by passing air through the mandrel. The resulting mechanically strained member is measured by triangulation laser. Patterned collapsible (auxetic) tessellations are calculated over this double curved inflated surface and converted to computer

numeric control toolpaths. Multiple layers of a hard (Shore 73A) silicone is extruded over and bonded to the stretched substrate. When the entire structure has crosslinked and bonded together, the compressed air is removed. The structure deflates, transferring strain energy from the membrane to extruded frame, until settling in a minimum energy form. Petralia *et al* [2] gave an in-depth description of DEMES fabricated by laminating 2D planar layers under differing levels of tension and compression and allowed to buckle out-of-plane. These out-of-plane buckled structures were described as difficult to model; particularly when trying to anticipate their resting shape in minimum energy form. In part, this was because the hand-made aspects of these structures resulted in non-uniform strain being applied to the hand stretched membranes. This was exacerbated by application of an arbitrary shaped pliant planar frame to that membrane. Building on their concept, it is the desire of this series of papers to demonstrate DEMES using custom fabricated balloons with extruded auxetic support frames which collapse in a more regular and predictable way. Spray deposition of PDMS membranes via atomisation using pressurised air is discussed in [3]. Here silicone DEA were created by spraying dichloromethane diluted silicone (Sylastic 3481) onto the straight edge of a rotating wheel. Long tape like membranes of consistent thickness ranging from 40 µm to 160 µm were created. The authors discussed the principles of using overlapping spray lines to create a constant membrane thickness over a wide but flat area. The paper presented here seeks to investigate how to go further by spraying on double curved rotating surfaces. Planar PDMS pattern creation by airbrush was also discussed in [4]. Fabrication of tubular membranes for dielectric elastomers via dip coating was proposed in [5] & [6]. Pre-stretching an elastomer membrane increases the surface area while reducing the thickness. The result is stored strain energy in the elastomer, along with at thinning of the membrane. The change in material properties resulting from pre- stretch, known as stress softening or the “Mullins effect” is discussed and tested in [7]. Elastic strain energy from stretching tends towards returning to its un-stretched state if not constrained in some way. Methods to hold a strained elastomer from collapse included wrapping around a compressed spring [8], pliant incompressible planar frames [8], conical diaphragms [9], shell-like actuators [10] and inflated balloon-like implementations [11]. Beyond adding elastic energy, it has been shown that pre-stretch increases the dielectric breakdown strength by up to one order of magnitude [12], [13]. This is particularly important in the fabrication of DEA. Balloon actuators were created in [11] & [14] byrolling up and gluing of planar elastomer membranes into cylinders, then inflating with a hose. Such fabrication methods are seen as sub-optimal, due in part to the presence of and the inherent weakness of seams; this prevents achieving high levels of pre-strain without the ‘balloon’ rupturing. Also, such seams inhibit the symmetrical equibiaxial growth of the balloon form during inflation. Arbitrary shaped balloons were created using casting methods for spherical balloons using a five-part spherical mould [15]. Problems such as variation in membrane thickness of ±50 µm arose from the tolerances of the 3D printer used to fabricate the mould [16]. Flat pneumatic artificial muscles were created in [17], by pour casting flat sheets, and strengthening by embedded Kevlar fibres. This paper seeks to form a balloon as a single membrane using an additive manufacturing aerosol process. The only requirement is a positive mould (mandrel) upon which to deposit the membrane. This mandrel is fabricated to be air permeable, so it can act as an inflation mechanism, and therefore act as a departure point for balloon inflation. This obviates seams and allows for much greater flexibility in initial balloon shape. Emphasis is put on creating the smoothest surface mandrel with highest porosity possible – this encourages equal strain softening on all parts of the balloon membrane during inflation,

thus resulting in the most axially symmetric inflated substrate as possible. There are a number of materials from which a permeable inflating mandrel can be created: sintered metal or glass powder, porous polymer or mineral substrate. Perhaps the quickest method with lowest cost is achieved by casting the mandrel from mineral calcium sulphate (gypsum). The porous properties of the crystallised hemihydrate form of calcium sulphate have long been known and are well defined. A method described in [18] discusses persistent permeability in a plaster body. The authors state that it is preferable to utilise a minimum of water in the plaster mix for the most porous and the longest wearing gypsum preparation. This makes the material more difficult to handle when casting. Instead, an excess of water is generally used in order to remove air bubbles and achieve a superior surface finish. The excess water, i.e. water not required for the conversion reaction from hemi- hydrate to the dehydrate form is referred to as “held water” due to its retention in the crystallised matrix. The authors found that when compressed air was injected into the centre of the main body (core) of the mould, it forced most of the held water to percolate out to the surface. This imparted a significant permeability to the final body. It was necessary to carry out this procedure after the ‘initial set’, but before the ‘final set’ when the gypsum reached stable crystallisation. Both α and β forms of gypsum can be used; both of these will then exhibit a stable and permanent permeability and a marked improvement in the stabilisation of the outer surfaces against structural deterioration.

Materials and Methods

Fabrication of a permeable mandrel

To create a mould for casting the gypsum mandrel, an axially symmetric ‘cigar’ shape was drawn on CAD and produced on a CNC lathe using Necumer M1050, a high density polyurethane ‘chemiwood’ (Figure 1(b)). This shape was chosen arbitrarily. The shape was used as a mandrel ‘positive’, i.e. a positive form was cast, allowing creation of a seamless single sleeve negative mould into which gypsum could be poured to create a permeable mandrel. The sleeve mould was composed of a low Shore hardness silicone. (Smooth-On Ecoflex 00-30). This is shown in Figure 1(f). The mandrel itself was built in co-axial layers – shown schematically in Figure 1(a). The core was created from 6 mm (OD) 4 mm (ID) mild steel tubing with its mid-section (one third) removed. This gap was bridged by ‘Molduct’ porous tubing (a porous cellulose and cotton woven tube). Cyanoacrylate glue was used to bond the Molduct to the steel then sealed with heat-shrink tube, as seen in Figure 1(c). An M3 screw thread was tapped into either end of the steel tube, allowing pneumatic fittings to be attached. The porous Molduct section is the zone from which the inflation pressure emanated. Applied pneumatic pressure created pores in the mandrel which radiated out towards the outer forming surface of the gypsum body. By controlling the length and position of the Molduct, it was possible to specify which area of the mandrel surface became permeable. To reinforce the gypsum body, a tubular monofilament biaxial braid (Techflex Flexo PPS) was pulled loosely over the core and adhered at the ends, as seen in Figure 1(d).

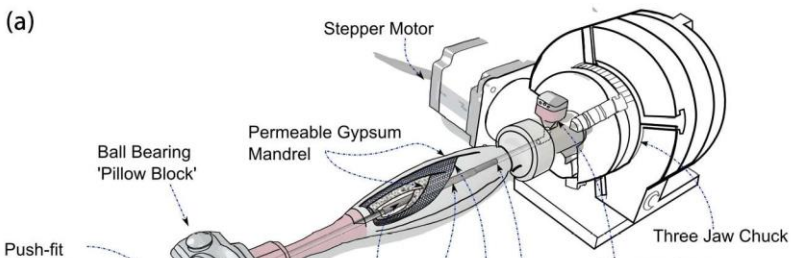

Figure 1 (a) Schematic of Mandrel assembly including cutaway illustrating internals (b) Chemi-wood mandrel positive (c) Mandrel Core - axis and permeable section (d) Core including biaxial braid (e) Silicone mould in tube, filled with gypsum (f) Set gypsum mandrel being demoulded (before purge cycle)

The steel and Molduct core, and braid assembly were inserted into the silicone sleeve mould, and kept aligned along the axis using a custom jig. Figure 1(e) shows the mould after the gypsum was poured in, and Figure 1(f) depicts the mandrel removal from the mould after it had set hard. Gypsum was prepared in excess of what was needed for casting, and a thermometer probe was inserted into the leftover material. The temperature was monitored during the exothermic phase – corresponding to crystallisation. At the point where temperature reached a maximum and then began to fall, the gypsum was considered to have hit 'initial set', and all the water required for crystallisation had been taken up. This does not occur at a definite temperature or time – it depends on ambient temperature and that of the water used. In these experiments, the water was chilled to 6˚C before use, to minimise variation. When Alpha

gypsum was tested it had a pour time between 6 and 8 minutes and initial set time between 30 and 35 minutes. Beta gypsum was considerably slower to crystallise, remaining pourable for up to 15 minutes, and setting at approximately 45 minutes. At the point of full crystallisation, pressurised air was driven into the core of the plaster body to remove any held water not required for the reaction; this is termed the 'purge cycle' and is depicted in Figure 2(a). Initial purge pressure was kept low, beginning at 70 kPa and then slowly increased by 35KPa every five minutes over the course of an hour to 480 kPa. A complete mandrel including a core pressure sensor at the proximal (motor) end, and pneumatic fitting and centring bearing at the distal end is shown in Figure 2(b). Figure 2(c) and 2(d) compares what is considered a poor and good resulting mandrel surface (respectively) after the purge cycle.

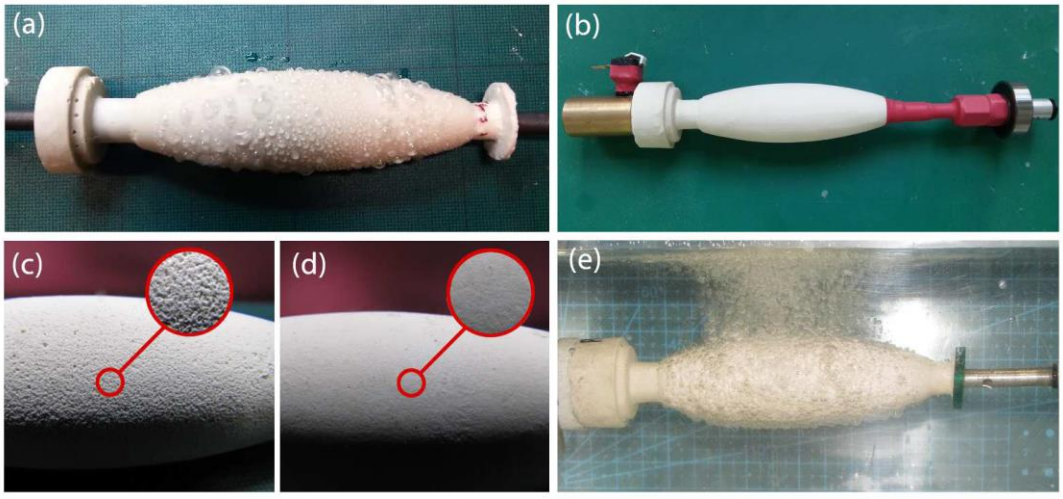

Figure 2 (a) Mandrel during purge cycle showing excess water being removed (b) Complete assembled mandrel, including push fit input valve and ball-bearing race at the distal (right) end, and core pressure sensor at the proximal (left) end. (c) Rough surface after purge, due to excessive initial purge pressure (d) Smooth post-purge mandrel. (e) Air being put through submerged permeable mandrel.

When the purge cycle was complete, the resulting final body was a highly and persistently permeable mandrel with pores of approximately 1 µm [19]. Figure 2(e) shows the mandrel submerged in water with compressed air driven through the surface.

Testing of Mandrel Permeability

A number of methods were investigated to ascertain if a reduction in pressure differential between core and surface was readily attainable. This was to allow maximum control over the inflation. Two different types of gypsum were tested – a high density plaster with high Alpha-hemihydrate content (LaFarge Presta Form) and a low density, predominantly Beta-hemihydrate plaster (SaintGobain Pottery Plaster). The Presta Form has a Brinell Hardness of 150 N/mm^2. When the recommended Water to Plaster Ratio (WPR) of 37% by weight was used, the resulting body had a (pre-treated) porosity of 15% [20]. The Pottery Plaster had a recommended WPR of 68%, resulting in a Brinell hardness of 20 N/mm^2 and a porosity of 44% [21]. These two forms of gypsum are at either end of the available spectrum in terms of hardness and porosity. It is worth noting that the porosity quoted does not guarantee true permeability. In addition to testing the two materials in their recommended form, variations were made in the WPR, together with the initial and incremental pressures used during the purge cycle to test

whether higher initial water content would result in a more porous final body. This assumption came from the observation that the gypsum body does not shrink during crystallisation when a high WPR is used, therefore the crystal structure must be less dense. Additionally, it was supposed that a faster purge cycle may remove more held water before final set, thus increasing final permeability. A test was performed to ascertain if the removal of trapped air bubbles would result in a better surface, without negatively affecting permeability. Here, fresh mixed gypsum was poured into the mould, and then vacuum degassed (Christ Alpha 1-2 LDplus Freeze Dryer). Pressure was reduced to 100mbar at room temperature and then released. A test setup was constructed to measure the pressure drop between the core and surface of the plaster with various mandrels. The setup (Figure 3) consisted of a 350 ml high density polyethylene (HDPE) tubular container, with a pressure sensor (Honeywell 40pc100g) fitted and sealed at one end to measure the pressure on the outside of the mandrel. The mandrel to be tested was inserted into the tube, and sealed at the other end using a silicone stopper with two 4 mm pneumatic pipes through it. Two pneumatic pipes were connected to either end of the mandrel. One of these pipes was connected to a second pressure sensor, used to measure the pressure in the core of the mandrel. The other was connected to a 3/2 way valve through which pressurised air could be controlled (and vented). Air pressure was digitally controlled using a Festo VPPE digital air pressure controller.

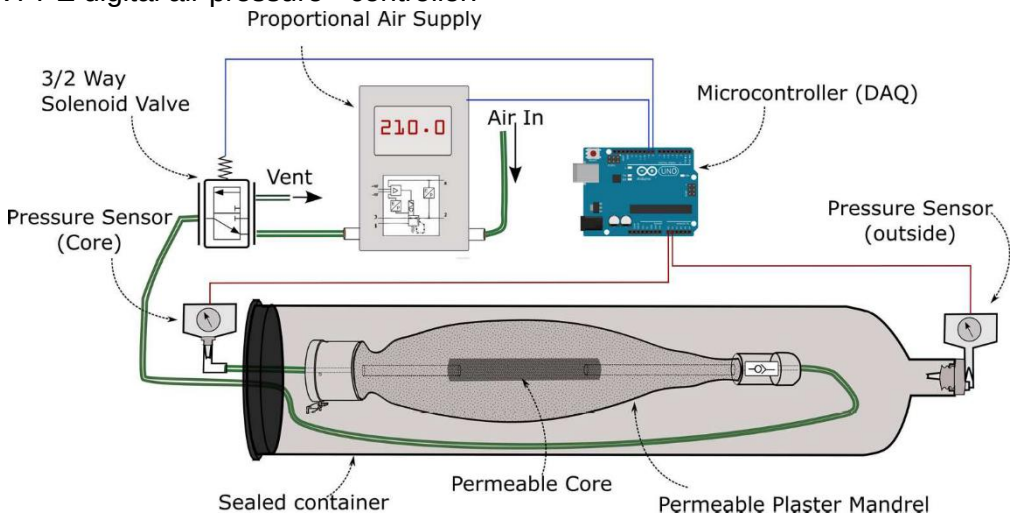

Figure 3 Test setup to evaluate mandrel permeability

Spray Deposition on Mandrel

Spray coating the mandrel was accomplished using an atomising nozzle mounted on the 3D printer (Figure 4). The printer gantry (BFB-3000) was modified by removing the hot plastic extrusion nozzle and replacing it with a spray valve (Techcon TS- 5540) along with removing the proprietary control circuitry and replacing with an open source RAMPS system. The schematic in 4(a) shows the direction of the X, Y, Z and θ axes and a photograph of the spray system is shown in 4(b) and curing of a membrane using IR is shown in 4(c). This spray system can be thought of as analogous to an additive lathe. The major operating difference with this machine when compared to a subtractive one is the inability to dwell in one position (with the spray valve open) without negatively affecting the surface thickness homogeneity or introducing subsurface air bubbles.

Moving the spray head too slowly along the mandrel or with too high a material output will also result in an uneven surface deposition.

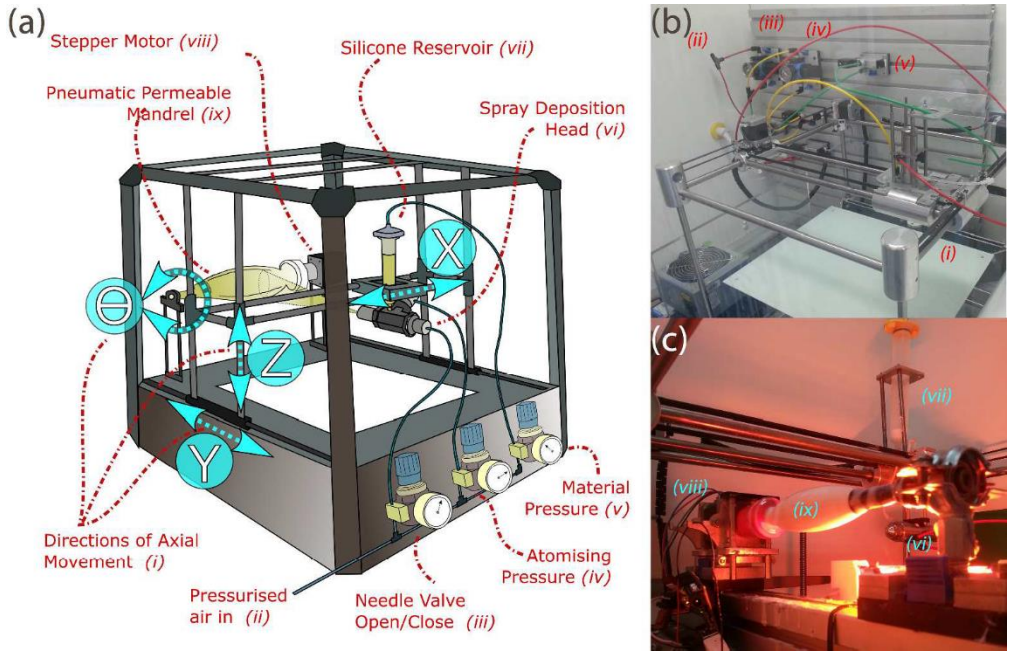

Figure 4 (a) Schematic of spray system, including direction of axes. (b) Actual spray gantry (c) Internals of spray system, showing sprayed membrane being cured using an Infra-red lamp.

The parameters: material and atomising pressure, along with needle valve open/close operations were controllable by individual pressure regulators with solenoids attached. The permeable mandrel assembly illustrated in Figure 1(a) was fixed at one side of the printer, lengthways to the spray valve. The method used to ensure even coverage of material was a 'constant angular velocity' approach (CAV). This is where the mandrel was rotated at a constant angular velocity ω, while the spray head moved at a variable speed V_{xy} while at a constant distance from the substrate. To achieve CAV, the spray carriage was moved at a speed inversely proportional to the mandrel radius r at that point. The net result is that the spray head spends the same amount of time over any particular area of mandrel surface, regardless of the radius at that particular cross section.

Testing of solvents and spray valve parameters

The spray valve used – Techcon TS-5540 with 1.17 mm nozzle – had a quoted maximum material viscosity of 10,000 mPa·s. The material used was Smooth-On Ecoflex 00-30, with a mixed viscosity of 6,000 mPa·s. When sprayed in undiluted form, the elastomer did not atomise well. It required very a high atomising pressure and it formed large droplets that agglomerated on the substrate. The material eventually slumped and merged, but this happened in an extremely random and uneven manner. It was felt that a solvent was required to achieve an even coating. Lotoxane (Arrow Chemicals), an aliphatic hydrocarbon solvent, was mixed with the silicone at 15% by weight. This reduced the silicone viscosity to 1800 mPa·s. Even at this reduced

viscosity, a reasonably high atomising and material pressure was required to create a consistent spray pattern (these pressures were kept equal). Through initial experiments, pressures greater than 200 kPa were found to be preferable for creating a homogeneous layer thickness without the material 'spitting' from the valve. At such pressures it was necessary to keep the deposition nozzle at a distance of at least 80 mm from the substrate. Anything closer tended to leave a central furrow in the deposited line. After initial test observations, parameters were refined and an experiment (n=36) was conducted to determine the effects of spray head speed along the linear axis, constant rotation speed of mandrel, material and atomising pressure, distance of the mandrel from substrate and the number of spray passes. The latter was a test to determine if the application of a second layer before the first had fully vulcanized would improve layer consistency.

Some non-sensible combinations such as high material pressure at close distance were discounted, as was a low rotation speed with fast linear print carriage speed (which would result in a non-overlapping helix of material being deposited). A subset of the factor combinations was chosen where some of the combinations were replicated, thus allowing error to be determined following statistical analysis by multiple regression. Table 1 shows the upper, middle and lower values of the test parameters. After each sprayed layer was cross-linked, the top surface was dusted with graphite, to help delineate the layers while measuring.

Table 1 Extent of test parameters

	Head Speed (mm/min)	Rotation Speed (RPM)	Pressure (kPa)
Lower	1600	75	200
Middle	2400	150	250

When the experimental sprayed silicone films had hardened, they were removed from their mandrel and sectioned to allow the thickness of the layer to be measured. Sections were cut at intervals of 10 mm along the length of the 'balloon'. To ensure all cuts were made with a precise cross section every time, a sacrificial mandrel was put in place of the gypsum one. In this case a root vegetable (carrot) was pared to resemble the original mandrel shape then inserted into the silicone films. Cutting was performed in a single cut with a chef's cleaver. The thickness of every layer on each cross section was measured three times, each 120˚ apart using the measurement microscope in a FujiFilm Dimatix DMP2600.

Results and Discussion

The Mandrel

Tests conducted with the two forms of plaster at different WPR and purge pressures were designed to measure air percolation rate through the mandrel body. This was performed by recording the time taken for pressure to equalise between the inside (core) and the outside (surface) of the mandrel - as per Figure 3. Variables tested are shown in Table 2.

Table 2: Fabrication variables for mandrels

	Plaster Type	WPR	Initial Purge Pressure	Purge pressure increment / tim
Test 1	Form	37%	70kPa	35kPa / 5 min
Test 2	Form	45%	70kPa	35kPa / 5 min
Test 3	Potters	68%	70kPa	35kPa / 5 min
Test 4	Potters	72%	70kPa	35kPa / 5 min

The experiment involved recording the core and the surface pressures of the mandrel every 100 ms for a total of 50 seconds while the core was exposed to an initial pressure of 210 kPa. The core pressure was then vented allowing the surface pressure to percolate back through the mandrel. The core and surface pressures are plotted against time (Figure 5) using dashed and dotted lines respectively. The differential pressure across the sensors is plotted using solid lines. The difference in pressure between the core and surface measurements – ΔP – was statistically analysed; the summary statistics are shown in Table 3.

Table 3: Statistics on Pressure Difference between inside and outside mandrel (Δ) at 210kPa

Pressure (210kPa)	Mean ΔP (kPa)	St Dev (kPa)	Median ΔP (kPa)	Q3 ΔP (kPa)	Max ΔP (kPa)
Test 1	45.7	44.2	28.13	69.8	179.2
Test 2	40.6	41.8	22.82	62.8	168.8
Test 3	18.0	27.1	3.03	24.1	123.7
Test 4	10.2	17.7	1.31	10.5	86.39

These consist of the mean ΔP, standard deviation of ΔP, median of ΔP and Q3 ΔP (i.e. the pressure difference above which one quarter of the readings lay) and Max ΔP, the maximum pressure difference between the core and the outside. Measurements: ΔP < 7 kPa (↑) (sec) and ΔP < 7 kPa (↓) (sec) represent the time in seconds for the pressure difference to drop to 7 kPa when pressure is increasing and decreasing respectively.

Experimentally, it was found when casting with LaFarge Form plaster, a very high WPR (>50%) results initially in a smooth glass-like surface. Ultimately, it was not a practicable way to

achieve a quality casting. The surface degraded significantly at the higher pressures used near the end of the purge cycle; similar to that shown in Figure 2(c). The same material at WPR of 45% gave a good balance of reduced viscosity for pouring without reducing the structural integrity required for a successful purge cycle. Due to the low WPR required – and therefore short working time – it was not possible to pre-process the slurry using methods such as vacuum degassing. Vibration during casting helped the migration of any trapped air up to the surface, resulting in a smooth final surface Figure 2(d) and Figure 2(b). When the mandrel is composed of 'Prestia Potters' beta plaster, it can be seen in Table 3 that the pressure differential between the outer and inner surface is significantly less than with 'Form' alpha plaster. The time taken for the two surfaces to equalise is also much shorter – as little as half the time. This increase in responsiveness comes at the cost of surface quality. The high pressure required at the end of the purge cycle tends to erode the surface. Using fine (1800 grade) sandpaper on the surface (during, but near the end of purge) will somewhat mitigate this, but doing so is only possible when the mandrel is a simple shape, as in this case.

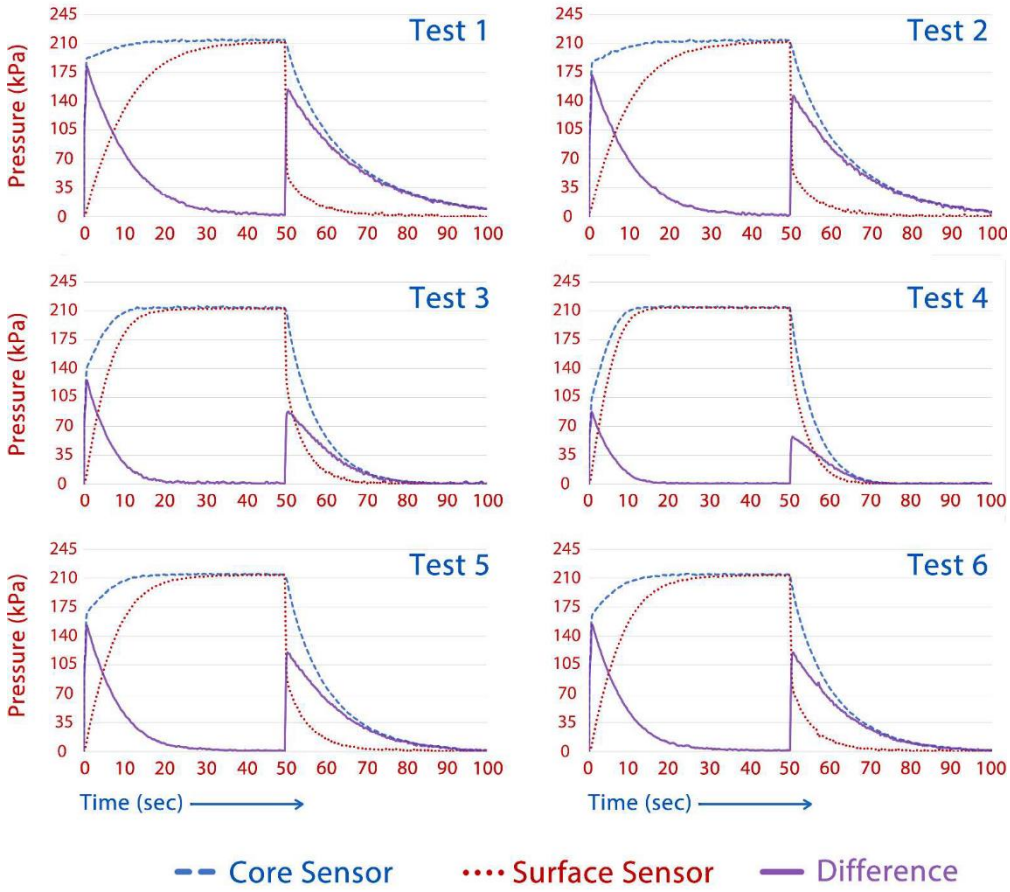

Figure 5. Pressure differences between core and surface of mandrels of varying types. Dashed line represents sensor readings from core of mandrel, dotted line representing the surface, and solid line shows the differential pressure.

Vacuum degassing does help remove trapped air bubbles at the interface with the mould, but not any more successfully than using vibration. A degas step reduces permeability also.

Spray Test

Regression analysis (Table 4) was undertaken to relate the mean thickness of each layer to head speed, rotation speed, pressure, distance of the head from the mandrel surface and number of passes of the spray jet. These were assumed to be the main factors that influenced the spraying of medium viscosity elastomers. The coefficient of determination (R^2) of 0.68 shows that the regression line fitted the measured data points very well. This can be seen by examining a scatter plot of measured vs predicted thicknesses (Figure 6(a)). The statistical significance of the F ratio (regression mean square/error mean square) is very high – the probability ≈ $2x10^{-6}$ demonstrates that the results could not reasonably have been arrived at by chance. Head speed was found to be the dominant factor influencing the evenness of coating at differing mandrel radii, thus faster head speed resulted in a smaller variability in thickness -see Figure 6(c).

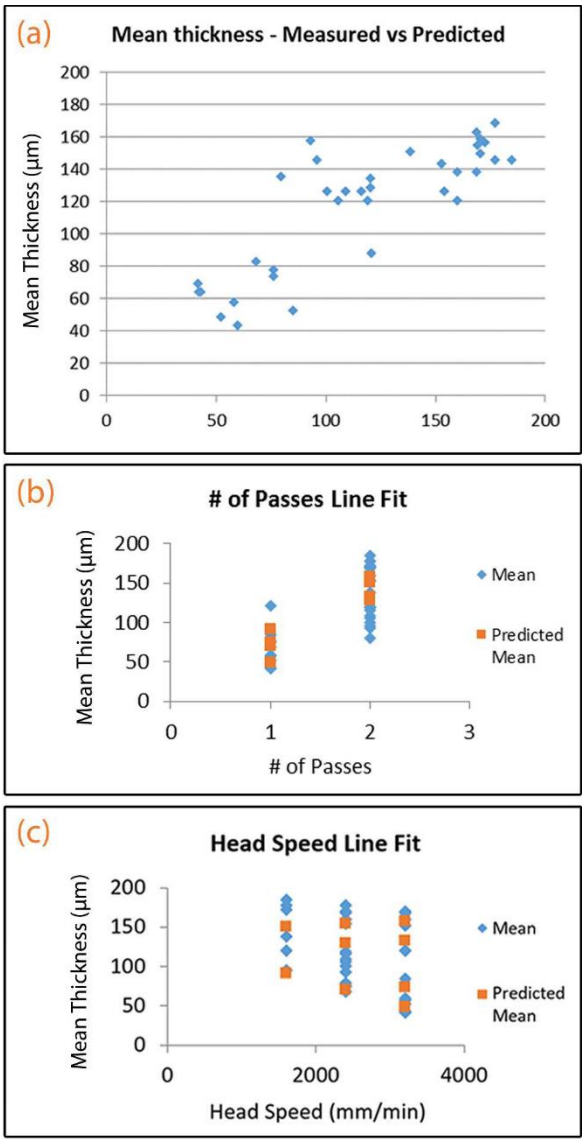

Figure 6: Regression Plots (a) Measured Vs Predicted layer thickness (b) Thickness of layer to number of passes (c) Thickness to head speed traveling along mandrel axis

Table 4: Regression analysis for measured thickness

Regression Statistics	
Multiple R	0.825
R Square	0.681
Adjusted R Square	0.626
Standard Error	28.319

	d	S	M	F	Significa F
Resid	29.000	23256.242			
Tot	34.000				

Variable	Coefficients	Err
Head Speed	-0.031	0
Rotation Speed	0.003	0
Pressure	55.261	22
Distance	-0.231	0
# of Passes	85.418	11

Examination of the calculated probability values (Table 4) shows that the variable 'number of passes' was the most significant factor in determining the thickness of the layer. This is not surprising, as a second pass will double the deposition time for any single area. Head Speed and Pressure are of lesser significance, but still important factors. All three have p-values of less than 0.05, thus allowing the null hypothesis to be rejected for these variables. Single variable plots for number of passes and head speed are presented in Figure 6(b) and (c). Pressure is not shown as a single-plot as alone its effect was not significant; however the effect of pressure may have been confounded with other factors arising from an incomplete dataset where all combinations of variables were not included. Rotational speed appears not to influence the layer thickness at the specific angular velocities tested. This was shown by a 49% probability coefficient. Figure 7(d) and (e) are graphs that show the mean sampled layer thickness of a sprayed membrane; each thickness is an average of fifteen measurements. These were measured at five different cross-sections on the tube spaced 10 mm apart. Figure 7(d) shows the most consistent two layers for a single pass spray and two for a double pass, the parameters of which are shown in Table 5

Table 5: Standard Deviations for the 'best' two single and double pass layers

	Head speed (mm/min)	Rotation speed (RPM)	Pressure (kPa)	Distance (mm)	Pas
THINNEST ACHIEVED LAYERS. Graph - Figu					
Two Pass Series 1	2400	75	250	80	
Two Pass Series 2	2400	150	200	80	
Single Pass Series 1	3200	150	300	150	
Single Pass Series 2	3200	150	300	150	
REPEATIBILITY OF SPRAY. Graph - Figure					

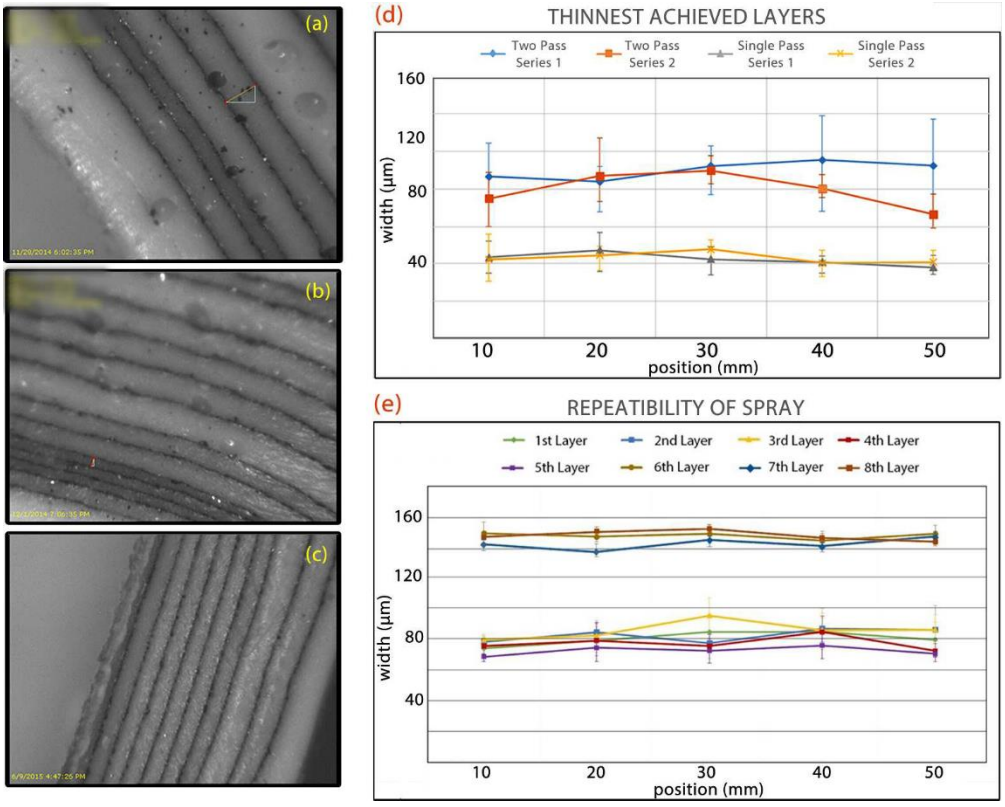

Figure 7: (a) and (b) Microscope imagery of cross sections corresponding to testing to find thinnest consistent layers. (c) Image of cross section corresponding to repeatability of sprayed layers. (d) Graph showing thickness of layers with maximum and minimum deviation. (e) Graph showing thickness of layers, when parameters were kept constant and layers repeated.

Examination of the curves shows that the best layers created with two passes display large variation in thickness, and have large error bars. Not shown in the graph is the large number of trapped air bubbles in the layers; these are clearly visible in Figure 7(a) and (b). In contrast, the best two single pass membranes are more satisfactory in their uniformity and standard error. Figure 7(c) shows repeatability in the thickness of layers when holding the spray parameters constant and applying layers on top of each other. Layers 6 to 8 in this series represent a two pass spray, but in this case the first layer is vulcanised before the second is applied. Using this technique, the standard error and uniformity are improved, without introducing air bubbles.

Inflation of membranes and simple deposition printing

Balloons were prepared by depositing 8 single pass layers at the optimal parameters – as per Table 5 and Figure 8(c). This resulted in a series of balloons with an average wall thickness of 560 µm (uninflated). The final inflated shape of four different balloons is shown in Figure 8(a-d). The first two, (a) and (b), were sprayed onto mandrels composed of the softer Beta plaster. They show an obvious lack of axial symmetry which resulted from the adherence of the silicone membranes to the mandrel during inflation due to surface roughness. The second pair, (c) and (d) were much more satisfactory – due to the use of smoother surface mandrels made of alpha gypsum. It is significant that non symmetric balloons will display a variation in stress softening across the surface of the membrane, and will repeatedly inflate in this non-symmetrical manner. It is noticeable that while the inflated membranes in Fig 8 (c) and (d) are both relatively symmetrical axially; they display a different overall profile shape along the axis. This is despite all spray parameters being identical for both pieces. Figure 8(e) and (f) show balloons inflated after Shore 30A hardness thixotropic silicone (Smooth-On Mould-Max 30, with 3% Smooth-On ThiVex additive) had been 3D printed upon them – one longitudinally and one co-axially. This demonstrates an ability to vary the final inflated shape without changing the mandrel design. Figure 8(e) and (f) respectively show balloons with longitudinal and co-axial lines printed on them before inflation. Figure 8(g) shows an inflated balloon with a zigzag pattern printed over its stretched surface and (h), the same balloon deflated, illustrating variation of strain across the surface of the membrane. The methods used to 3D scan the dimensions of the balloon substrate and then calculate constant line thickness toolpaths over the curve-linear surface are discussed in Part II of this series.

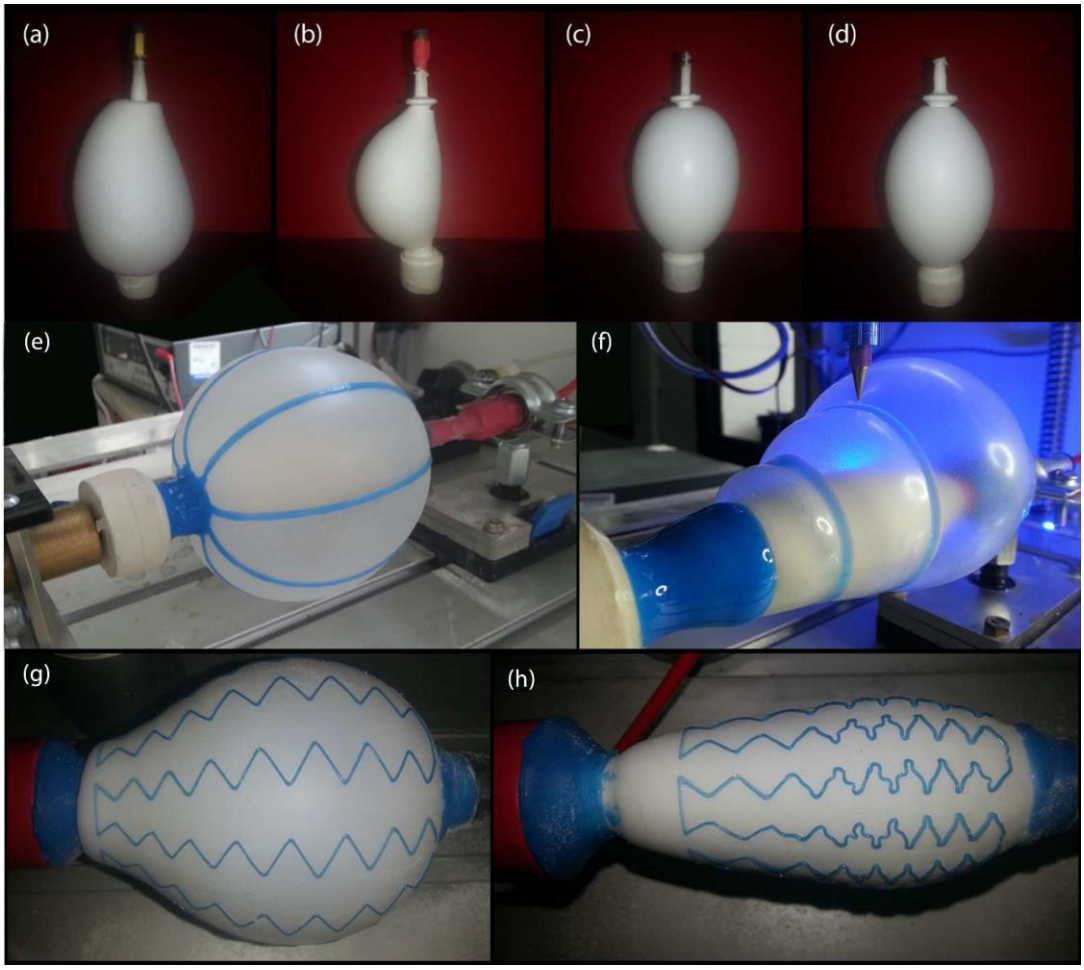

Figure 8: (a)(b) Inflated balloons which had been sprayed onto mandrels with poor surfaces, resulting in non- symmetric inflation (c)(d) Axially symmetric inflation of balloons (e) Balloon with longitudinal lines printed on it before inflation (f) Balloon with co-axial lines printed in it before inflation. (g) Inflated balloon with zig- zag pattern printed over stretched surface (h) same balloon deflated, illustrating variation of strain across the membrane.

Conclusions

The Mandrel

Pneumatically treated gypsum provides a low cost and flexible method with which to create permeable mandrels. Defects on the mandrel surface are detrimental to the quality of a fabricated balloon. When silicone is sprayed onto the mandrel, it flows into any holes creating 'anchors' which tend to constrain a point of the membrane to the surface during inflation, thus causing non-axial symmetry in the inflated shape. Using a hard predominantly, alpha-gypsum material to fabricate the mandrel results in an overall smoother final surface. However, it also requires a much higher inflation pressure at the mandrel core. The softer and more permeable beta-gypsum based mandrels need lower pressure but tend to suffer from a shorter useable life. For this reason, alpha-gypsum is preferable in most cases.

Spraying

Spray deposition of multiple silicone membranes layers onto an air-permeable mandrel followed by inflation is a viable way to create balloons with an axially symmetric inflated shape. With spray deposition of silicone on to complex curved surfaces, variation in deposited membrane thickness is undesirable, so when spraying a high viscosity material, it is best:

(a) to use a relatively high atomising and material pressure of 300 kPa,
(b) to keep the spray jet at 120 mm from substrate and
(c) to traverse the print- head quickly along the axis at 3200 mm/min.

Thickening of the layers sometimes occurs towards the mid-point of the mandrel. This may be a consequence of the greater diameter (Z-width) at the centre of the mandrel or of the tendency of the circular spray beam to deposit more material at the centre. The slightly thicker layer may confer an advantage during inflation, as the material at the midpoint of the mandrel is subjected to a higher level of strain during inflation, thus becomes thinner. Spraying a thin layer and then curing, followed by depositing a second layer improves variability significantly. The 'double layer' approach does result in membranes with thicker walls, but this is countered by the thinning of the membrane during inflation. The techniques described in this paper have applications in fields such as soft robotics, particularly dielectric elastomer actuators. Beyond this, the authors see uses within 3D printing of tubular and non-planar objects with removable substrates, uses in stretchable electronics and 4D printing of objects with multiple varying levels of mechanical strain throughout the object.

Corresponding Author :

Fergal B Coulter
Department of Mechanical and Materials Engineering
University College Dublin
Belfield
Dublin 4
Ireland
contact@fergalcoulter.eu

Author Disclosure Statement :

All experimental work was completed at, and funded by Nottingham Trent University, School of Architecture, Design and Built Environment. There is no conflict of Interest.

References

[1] Coulter; F B. and Ianakiev; A., (2015) 4D Printing Inflatable Silicone Structures, 3D Printing and Additive Manufacturing. 2(3): 140-144.
[2] Petralia, M.T.; Wood, R.; (2010) Fabrication and analysis of dielectric-elastomer minimum-energy structures for highly-deformable soft robotic systems, Intelligent Robots and Systems (IROS), 2010 IEEE/RSJ International Conference on, pp. 2357–2363, 2010
[3] Araromi; O.A., Conn; A.T., Ling; C.S., Rossiter; J.M., Vaidyanthan; R., Burgess; S.C., (2011) Spray deposited multi-layered dielectric elastomer actuators. Sensors and Actuators A 167(2011) pp 459-467
[4] Chooneea, K; Syms R.R.A.; Ahmada, M.M.;. Zoub, H; Post processing of microstructures

by PDMS spray deposition. Sensor and Actuators A, 155 (2009) 253–262
[5] Pelrine; R.E, Kornbluh; R.D., Joseph; J.P. (1998) Electrostriction of polymer dielectrics with compliant electrode as a means of actuation. Sensors Actuators A 64 pp77-85 (1998)
[6] Carpi; F., De Rossi; D, (2004) Dielectric elastomer cylindrical actuators: electromechanical modelling and experimental evaluation, Materials Science and Engineering: C, Volume 24, Issue 4, 1 June 2004, pp 555-562.
[7] Johnson; M.A., Beatty M.F. (1995) The Mullins effect in equibiaxial extension and its influence on the inflation of a balloon. International Journal of engineering science, Vol 33, No. 2 pp 223-245.
[8] Zhang R; Lochmatter, P; Kunz, A; and Kovacs G. (2006) Spring Roll Dielectric Elastomer Actuators for a Portable Force Feedback Glove. Smart Structures and Materials 2006: Electroactive Polymer Actuators and Devices (EAPAD), Proceedings of SPIE Vol. 6168, 61681T.
[9] Rossiter, J; Walters, P.; Stoimenov, B; (2009) Printing 3D dielectric elastomer actuators for soft robotics. Proc. SPIE 7287, Electroactive Polymer Actuators and Devices (EAPAD) 2009, 72870H
[10] Lochmatter, P. (2007) Development of a Shell-like Electroactive Polymer (EAP) Actuator. PhD Thesis. Swiss Federal Institute of Technology, Zurich.
[11] Soleimani; M., Menon C (2010) Preliminary investigation of a balloon shaped actuator based on electroactive elastomers. Smart Mater Struct. 19 (2010) 047001.
[12] Kofod; G., (2008) The static actuation of dielectric elastomer actuators: how does pre-stretch improve actuation. *J. Phys. D: Appl. Phys.* 41 (2008) 215405
[13] Plante J.S., Dubowsky S, (2006) Large-scale failure modes of dielectric elastomer actuators, International Journal of Solids and Structures, Volume 43, Issues 25–26, December 2006, Pages 7727-7751.
[14] Potz; M., Artusi; M., Soleimani; M., Menon; C., Cocuzza; S., Debei; S., (2010) Rolling dielectric elastomer actuator with bulged cylindrical shape. Smart Mater. Struct 19 (2010) 127001.
[15] Ahmadi; S., Gooyers; M., Soleimani; M., Menon; C., (2013) Fabrication and electromechanical examination of a spherical dielectric elastomer actuator. Smart Mater. Struct. 22 2013 115004
[16] Soleimani; M (2010) Development of a novel balloon shaped electroactive polymer (EAP) actuator. Master of Applied Science (Thesis). Simon Frazer University, British Coumbia, Canada.
[17] Park, Y.L., Santos, J., Galloway, K.G., Goldfield, E.C. and Wood, R.J., 2014, May. A soft wearable robotic device for active knee motions using flat pneumatic artificial muscles. In Robotics and Automation (ICRA), 2014 IEEE International Conference on (pp. 4805-4810). IEEE.
[18] Bryer and Steele (1949) Treatment of plaster molds. Patent US 2632209.
[19] Ceramic Industry Magazine (2000) Synthetic Molds Go Mainstream. Published November 2000
[20] Lafarge 2013 Prestia Form Datasheet: http://www.rbhltd.com/wp-content/uploads/2012/01/PRESTIA-FORM.pdf
[21] Saint Gobain Pottery Plaster datasheet http://www.saintgobainformula.com/tds/export/%28nid%29/19908